

# DISCOVERING AND EXPLAINING THE REPRESENTATION BOTTLENECK OF DNNs

Huiqi Deng, Qihan Ren, Xu Chen, Hao Zhang, Jie Ren, Quanshi Zhang\*

Shanghai Jiao Tong University

{denghq7, renqihan, xcheng8, 1603023-zh, ariesrj, zqs1022}@sjtu.edu.cn

## ABSTRACT

This paper explores the bottleneck of feature representations of deep neural networks (DNNs), from the perspective of the complexity of interactions between input variables encoded in DNNs. To this end, we focus on the multi-order interaction between input variables, where the order represents the complexity of interactions. We discover that a DNN is more likely to encode both too simple interactions and too complex interactions, but usually fails to learn interactions of intermediate complexity. Such a phenomenon is widely shared by different DNNs for different tasks. This phenomenon indicates a cognition gap between DNNs and human beings, and we call it a *representation bottleneck*. We theoretically prove the underlying reason for the representation bottleneck. Furthermore, we propose a loss to encourage/penalize the learning of interactions of specific complexities, and analyze the representation capacities of interactions of different complexities.

## 1 INTRODUCTION

The revolution from shallow to deep models is a crucial step in the development of artificial intelligence. Deep neural networks (DNNs) usually exhibit superior performance to shallow models, which is generally believed as a result of the improvement of the representation power (Pascanu et al., 2013; Montúfar et al., 2014). To this end, instead of considering previous issues of the accuracy and the generalization ability of DNNs, we focus on the following two questions about the representation capacity:

- Are there any common tendencies of DNNs in representing specific types of features?
- Does a DNN encode similar visual concepts as human beings for image classification?

In order to answer the above two questions, our research first investigates the bottleneck of knowledge representation, *i.e.*, which types of knowledge points (*e.g.*, certain visual concepts) are likely to be encoded by a DNN, and which types of knowledge points are difficult to be learned. To this end, we discover that the interaction between input variables is an effective tool to analyze the knowledge representation. It is because the DNN does not consider input variables working independently, but it encodes the interaction between input variables to form an interaction pattern for inference. For example, the inference of a face image can be explained as the interaction between left and right eyes, the interaction between nose and mouth, and etc.

As the answers to the above questions, we discover a common representation bottleneck of DNNs in encoding interactions, *i.e.*, a DNN is more likely to encode both too complex and too simple interactions, instead of encoding interactions of intermediate complexity. This also indicates a dramatic difference from human cognition.

The interaction can be understood as follows. Let us take the face recognition task for example. Let  $\phi_{i=\text{mouth}}$  measure the numerical importance of the mouth region  $i$  to the classification score. Then, the interaction utility between the mouth region  $i$  and the nose region  $j$  is measured as the change of the  $\phi_{i=\text{mouth}}$  value by the presence or absence of the nose region  $j$ . If the presence of  $j$  increases the importance  $\phi_{i=\text{mouth}}$  by 0.1, then, we consider 0.1 as the utility of the interaction between  $i$  and  $j$ .

\*Correspondence. This study is conducted under the supervision of Dr. Quanshi Zhang. zqs1022@sjtu.edu.cn. Quanshi Zhang is the corresponding author. He is with the John Hopcroft Center and the MoE Key Lab of Artificial Intelligence, AI Institute, at the Shanghai Jiao Tong University, China.

**Multi-order interactions.** In order to represent the interaction complexity mentioned in the representation bottleneck, we use the multi-order interaction utility between variables  $i, j$  proposed by Zhang et al. (2020). The interaction of the  $m$ -th order  $I^{(m)}(i, j)$  measures the average interaction utility between variables  $i, j$  on all contexts consisting of  $m$  variables. In this way, the order  $m$  reflects the contextual complexity of the interaction. A low-order  $I^{(m)}(i, j)$  measures the relatively simple collaboration between variables  $i, j$  and a few  $m$  contextual variables, while a high-order  $I^{(m')}(i, j)$  corresponds to the complex collaboration between  $i, j$  and  $m'$  massive contextual variables, where  $m' \gg m$ .

Moreover, we prove that the multi-order interaction is a trustworthy tool to analyze the representation capacity of DNNs. Specifically, the output score of a DNN can be decomposed into utilities of compositional multi-order interactions between different pairs of variables, *i.e.*,  $model\ output = \sum_{m=0}^{n-2} \sum_{i,j \in N, i \neq j} w^{(m)} I^{(m)}(i, j) + \sum_{i \in N} local\ utility\ of\ i + bias$ . For example, the inference score of a face can be decomposed into the interaction utility between left and right eyes, between mouth and nose, and etc. Therefore, we can take the utility  $I^{(m)}(i, j)$  as the underlying reason to explain the DNN, because each interaction makes a compositional contribution to the output.

**Representation bottleneck of DNNs.** Surprisingly, the above decomposition of multi-order interactions enables us to discover a representation bottleneck of DNNs. As Figure 1(b) shows, low-order and high-order interaction utilities  $I^{(m)}(i, j)$  usually have high absolute values, while middle-order interaction utilities  $I^{(m)}(i, j)$  usually have low absolute values. In other words, a DNN is more likely to encode the interaction between variables  $i$  and  $j$ , when  $i, j$  interact with a few contextual variables. Similarly, it is also easy for the DNN to learn the interaction, when  $i, j$  interact with most contextual variables. However, it is difficult for the DNN to learn the interaction, when  $i, j$  cooperate with a medium number of contextual variables. The difficulty of learning middle-order interactions reflects a representation bottleneck of DNNs.

**Cognitive gap between DNNs and humans.** Such a representation bottleneck also indicates a significant gap between the knowledge representation of DNNs and the visual cognition of humans. As Figure 1(c) shows, people usually cannot extract meaningful information from a few image patches. Besides, if people are given almost all patches, then the information is already too redundant and inserting additional patches will bring in little new information. In contrast, the DNN encodes most information, when the DNN is given only a few patches or is given most patches.

**Theoretical proof.** In this paper, we theoretically prove the mechanism that is responsible for the representation bottleneck. Such a proof also enables us to simulate the distribution of interactions of different orders, which well matches the distribution of interactions in real applications.

Beyond the theoretical proof, another important issue is how to guide the learning of knowledge representation in DNNs by learning interactions of specific orders. We propose two losses to encourage/penalize the DNN to make inferences by interactions of specific orders, thereby boosting/preventing the learning of such interactions. Experimental results have validated the effectiveness of the two losses. Next, we investigate the representation capacities of several DNNs which encoded interactions of different orders. We find that the DNNs mainly encoding high-order interactions represent more structural information than the normally trained DNNs. In addition, high-order interactions were vulnerable to adversarial attacks.

In summary, this paper makes three contributions:

- This study discovers a representation bottleneck phenomenon of DNNs, *i.e.*, it is difficult for a DNN to learn middle-order interactions. It also clearly proves that DNNs and humans use different types of visual concepts for inference.
- We theoretically prove the underlying reason for the representation bottleneck.
- We design two losses to encourage/penalize the DNN to learn interactions of specific orders. Experiments have validated the effectiveness of the proposed losses. Besides, we investigate the representation capacities of DNNs which encode interactions of different orders.

## 2 RELATED WORK

**The representation capacity of DNNs.** The evaluation of the representation capacity of DNNs provides a new perspective to explain and analyze DNNs. Pascanu et al. (2013) and Montúfar et al.

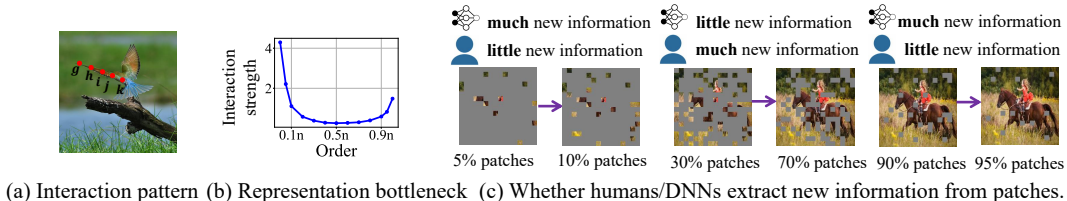


Figure 1: (a) Five pixels ( $g, h, i, j, k$ ) interact with each other, forming an edge pattern for classification. (b) Representation bottleneck. A DNN is likely to encode low-order and high-order interactions, but usually fails to learn middle-order interactions. (c) The cognition gap between DNNs and humans. Humans extract little information from a few image patches (e.g., 5% patches). Also, given almost all patches (e.g., 90% patches), the information is already redundant for human cognition. Then, people learn little new information from the additional 5% patches. In comparison, the DNN encodes most interactions when the DNN is given very few patches or most patches.

(2014) used the number of linear response regions in a deep rectifier MLP to evaluate its representation capacity. The information bottleneck theory (Shwartz-Ziv & Tishby, 2017) used the mutual information to explain how DNNs gradually learned the information during the training process. Achille & Soatto (2018), Amjad & Geiger (2019) and Hjelm et al. (2019) further improved the representation capacity by optimizing mutual information. Arpit et al. (2017) studied the memorization behavior of DNNs during training to analyze the feature representations. Xu (2018) proposed Fourier analysis to understand the generalization. In addition, several metrics were proposed to analyze the generalization capacity or robustness of DNNs, including the stiffness (Fort et al., 2019), the sensitivity (Novak et al., 2018), and the CLEVER score (Weng et al., 2018). Neyshabur et al. (2017) examined whether existing complexity measures can guarantee generalization.

Previous researches mainly studied the theoretically maximum complexity, generalization ability, and robustness of DNNs. In comparison, our research focuses on the limitation of DNNs in feature representations, *i.e.*, which types of interactions are unlikely to be encoded.

**Interactions.** Interactions between input variables of a DNN have been widely investigated in recent years. Based on the Shapley value (Shapley, 1951), Grabisch & Roubens (1999) proposed the Shapley interaction index to define the interaction in a cooperative game. Lundberg et al. (2018) used the interaction effect to build tree ensemble explanations for the decision of DNNs. Janizek et al. (2021) extended Integrated Gradients (Sundararajan et al., 2017) to explain the pairwise feature interaction in DNNs. Sundararajan et al. (2020) proposed the Shapley Taylor interaction to measure interactions among multiple variables. Tsang et al. (2020) and Tsang et al. (2017) interpreted DNNs by detecting statistical interactions between input variables and interactions between network weights respectively. Peebles et al. (2020) and Tsang et al. (2018) achieved the disentanglement of features by restricting interactions. Song et al. (2019) and Lian et al. (2018) designed network architectures to effectively learn feature interactions in the recommendation system. Lengerich et al. (2020) applied the ANOVA technique to model interaction effects and further explored the relationship between dropout and interactions. Zhang et al. (2020) proposed the multi-order interaction, and used it to understand and boost dropout. In this paper, we used the multi-order interaction to study the complexity of interactions encoded in DNNs.

### 3 REPRESENTATION BOTTLENECK

Before the analysis of the representation bottleneck, let us first introduce multi-order interactions between input variables, which are encoded in a DNN. Given a pre-trained DNN  $v$  and an input sample with a set of  $n$  variables  $N = \{1, \dots, n\}$  (e.g., an input image with  $n$  pixels),  $v(N)$  denotes the network output of all input variables. Input variables of DNNs usually interact with each other to make inferences, instead of working individually. In this study, we mainly discuss the pairwise interactions. For example, as Figure 1(a) shows, pixels  $i, j \in N$  interact with each other, forming an edge pattern for classification. If the existence of this pattern increases the network output by 0.01, we consider the *utility* of this pattern as 0.01. Similarly, if the existence of this pattern decreases the network output, we consider this pattern has a negative utility.

Furthermore, the multi-order interaction  $I^{(m)}(i, j)$  between two input variables  $i, j \in N$ ,  $0 \leq m \leq n-2$ , is proposed to measure interactions of different complexities (Zhang et al., 2020). Specifically, the  $m$ -th order interaction  $I^{(m)}(i, j)$  measures the average interaction utility between variables  $i, j$  under all possible contexts consisting of  $m$  variables. Therefore, the order  $m$  can be considered to represent the contextual complexity of the interaction. For example, as Figure 1(a) shows, five pixels  $(i, j, g, h, k)$  collaborate with each other and form an edge pattern for classification. Thus, the pairwise interaction between pixels  $i, j$  also depends on three contextual pixels  $g, h, k$ . Mathematically, the multi-order interaction  $I^{(m)}(i, j)$  is defined as follows:

$$I^{(m)}(i, j) = \mathbb{E}_{S \subseteq N \setminus \{i, j\}, |S|=m} [\Delta v(i, j, S)], \quad (1)$$

where  $\Delta v(i, j, S) = v(S \cup \{i, j\}) - v(S \cup \{i\}) - v(S \cup \{j\}) + v(S)$ . Here,  $v(S)$  is the output score when we keep variables in  $S \subseteq N$  unchanged but replace variables in  $N \setminus S$  by the baseline value. The baseline value follows the widely-used setting in Ancona et al. (2019), which is set as the average value of the variable over different samples. Let us take the multi-category image classification for example. Given an input image  $x$ ,  $v(S) = v(x_S)$  can be implemented as any scalar output of the DNN (e.g.,  $\log \frac{P(\hat{y}=y^{\text{true}}|x_S)}{1-P(\hat{y}=y^{\text{true}}|x_S)}$  of the true category), where we replace the pixel values in  $N \setminus S$  of original input  $x$  by the baseline value (the average pixel value over images) to construct a masked image  $x_S$ . Then,  $\Delta v(i, j, S) = [v(S \cup \{i, j\}) - v(S \cup \{i\})] - [v(S \cup \{j\}) - v(S)]$  measures the marginal interaction effects of the collaboration between  $i, j$  in a context  $S$ .

**Generic metric.** The proposed multi-order interaction  $I^{(m)}(i, j)$  is a generic metric, which has a strong connection with the Shapley value (Shapley, 1951) and the Shapley interaction index (Sundararajan et al., 2020) in game theory. In addition, it has been proven that  $I^{(m)}(i, j)$  satisfies the following five desirable properties, *i.e.*, **linearity**, **nullity**, **commutativity**, **symmetry**, and **efficiency** properties. The connections with existing metrics and five properties are introduced in Appendix A.

### 3.1 REPRESENTATION BOTTLENECK

According to the **efficiency** property of  $I^{(m)}(i, j)$ , we find that the network output of a DNN can be explained as the sum of all interaction utilities of different orders between different pairs of variables.

$$v(N) = v(\emptyset) + \sum_{i \in N} \mu_i + \sum_{i, j \in N, i \neq j} \sum_{m=0}^{n-2} w^{(m)} I^{(m)}(i, j) \quad (2)$$

where  $\mu_i = v(\{i\}) - v(\emptyset)$ , and  $w^{(m)} = \frac{n-1-m}{n(n-1)}$ . Because  $I^{(m)}(i, j)$  measures the interaction between variables  $i$  and  $j$  encoded in DNNs with  $m$  contextual variables, we can consider the interaction utility  $I^{(m)}(i, j)$  as a specific reason for the inference, which makes a compositional contribution  $w^{(m)} I^{(m)}(i, j)$  to the output.

In this way, we can categorize all underlying reasons for the network output into different complexities. Low-order interactions can be considered as simple underlying reasons, relying on very few variables. High-order interactions can be regarded as complex underlying reasons, depending on massive variables. In order to measure the reasoning complexity of the DNN, we measure the relative interaction strength  $J^{(m)}$  of the encoded  $m$ -th order interaction as follows:

$$J^{(m)} = \frac{\mathbb{E}_{x \in \Omega} [\mathbb{E}_{i, j} [|I^{(m)}(i, j| x)|]]}{\mathbb{E}_{m'} [\mathbb{E}_{x \in \Omega} [\mathbb{E}_{i, j} [|I^{(m')}(i, j| x)|]]]} \quad (3)$$

where  $\Omega$  denotes the set of all samples.  $J^{(m)}$  is computed over all pairs of input variables in all samples.  $J^{(m)}$  is normalized by the average value of interaction strength. The distribution of  $J^{(m)}$  measures the distribution of the complexity of interactions encoded in DNNs.

**Representation bottleneck.** Based on the above metric, we discover an interesting phenomenon: *a DNN usually encodes strong low-order and high-order interactions, but encodes weak middle-order interactions*. Such a phenomenon is shared by different DNN architectures trained on different datasets, which is illustrated by the  $J^{(m)}$  curves in Figure 2. Specifically, when the order  $m$  is smaller than  $0.1n$  or greater than  $0.9n$ , its interaction strength  $J^{(m)}$  is usually high. In comparison,  $J^{(m)}$  is usually low when the order  $m$  approximates  $0.5n$ . Moreover, as shown in Figure 3(a), we find that such a phenomenon does not only exist in the well-trained DNNs, but also exists in the entire network training process.

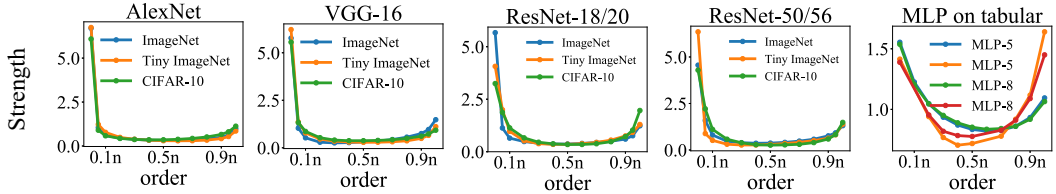


Figure 2: The distributions of interaction strength  $J^{(m)}$  of different DNNs trained on various image datasets and tabular datasets. Noted that the relative strength  $J^{(m)}$  of high-order interactions on two tabular datasets is higher than that on image datasets. This may be because that the classification on images usually depends on low-order interactions, but the classification on tabular data mainly depends on high-order interactions.

The above phenomenon indicates that a DNN is more likely to learn simple interactions where a few variables (*e.g.*, less than  $0.1n$  variables) interact with each other. Similarly, it is also easy for the DNN to encode the complex interaction where massive variables (*e.g.*, more than  $0.9n$  variables) interact with each other. However, it is difficult for the DNN to learn the middle-complex interaction in which a medium number of variables (*e.g.*, about  $0.5n$  variables) participate. Let us take Figure 1(c) for an example. When a DNN is given very few patches sparsely distributed on the horse image, the DNN can successfully extract the interaction between the few patches. Similarly, when the DNN is given almost all patches of the horse image, then the insertion of two new patches will make the DNN trigger strong collaboration between the two patches and massive existing patches. However, when the DNN is just given a half patches, it is difficult for the DNN to encode collaborations between two patches. In a word, the interaction pattern encoded by the DNN is either too simple or too complex. The difficulty of learning interaction patterns of moderate complexity reflects a common tendency in the feature representation in the DNN.

Such a representation bottleneck also indicates that DNNs and human beings encode different types of visual patterns for inference. As Figure 1(c) shows, (i) Given very few patches, a DNN can encode much information from low-order interaction patterns between patches. However, it is difficult for people to recognize such low-order interactions. (ii) Given almost all patches of an image, any additional patches are already too redundant for human cognition, so people do not obtain much new information from additional patches. (iii) Given a medium number of patches, the DNN usually extracts little information, while people can extract much information for recognition.

**Implementation details.** In order to measure  $J^{(m)}$ , we conducted experiments on three image datasets including the ImageNet dataset (Russakovsky et al., 2015), the Tiny-ImageNet dataset (Le & Yang, 2015) and the CIFAR-10 dataset (Krizhevsky et al., 2009). We mainly analyzed several DNNs trained on these datasets for image classification, including Alexnet (Krizhevsky et al., 2012), VGG-16 (Simonyan & Zisserman, 2014) and Resnet-18/20/50/56 (He et al., 2016). Due to the high dimension of input variables ( $n = 224 \times 224$  for ImageNet), the computational cost of  $J^{(m)}$  is intolerable. To reduce the computational cost, we split the input image into  $16 \times 16$  patches, and considered each patch as an input variable. To compute  $J^{(m)}$ , we set the network output as  $v(S|x) = \log \frac{P(\hat{y}=y^*|x_S)}{1-P(\hat{y}=y^*|x_S)}$  given the masked sample  $x_S$ , where  $y^*$  was the true label and  $P(\hat{y}=y^*|x_S)$  was the probability of classifying the masked sample  $x_S$  to the true category. In the masked sample  $x_S$ , pixel values in image patches in  $N \setminus S$  were replaced by the average pixel value over different patches in all images, just like in Ancona et al. (2019). Note that  $J^{(m)}$  is an average over all possible contexts  $S$ , all pairs of variables  $(i, j)$ , and all samples  $x$ , which is computationally infeasible. Therefore, we approximated  $J^{(m)}$  using a sampling strategy (Zhang et al., 2020). Please see Appendix C for sampling details. In addition, we conducted experiments on two tabular datasets, including the UCI census income dataset (census) and the UCI TV news channel commercial detection dataset (commercial) (Dua et al., 2017). Each sample in the two datasets contained  $n = 12$  and  $n = 10$  input variables, respectively. We analyzed a five-layer MLP (namely, MLP-5) and an eight-layer MLP (namely, MLP-8) network. Each layer except for the output layer contained 100 neurons. For each MLP network, we trained two models for the classification on the two datasets, respectively. In the computation of  $J^{(m)}$ ,  $P(\hat{y}=y^*|x_S)$  was also computed by setting the baseline value of a variable to the average value of the variable. Please see Appendix C for details.

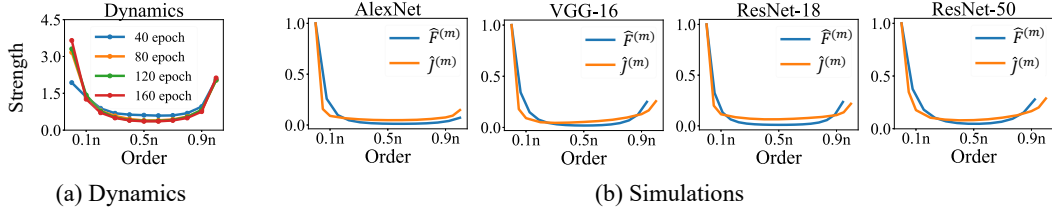


Figure 3: (a) Distributions of the interaction strength  $J^{(m)}$  of a ResNet-20 model over different orders, which are measured after different training epoches. The DNN is trained on the CIFAR-10 dataset. (b) Simulations of the  $\hat{J}^{(m)}$  distributions based on  $\hat{F}^{(m)}$  curves on the ImageNet dataset.

### 3.2 EXPLAINING THE REPRESENTATION BOTTLENECK

In this subsection, we theoretically prove the underlying reason for the representation bottleneck. Let  $W$  denote network parameters of a DNN. We focus on the change  $\Delta W$  of network parameters, which also represents the strength of training the DNN. The change of weights is calculated by  $\Delta W = -\eta \frac{\partial L}{\partial W} = -\eta \frac{\partial L}{\partial v(N)} \frac{\partial v(N)}{\partial W}$ .  $L$  denotes the loss function, and  $\eta$  is the learning rate. According to Eq. (2), the network output  $v(N)$  of the DNN can be decomposed into the sum of multi-order interactions  $I^{(m)}(i, j)$ . Therefore,  $\Delta W$  can be further represented as the sum of gradients  $\frac{\partial I^{(m)}(i, j)}{\partial W}$  of multi-order interactions.

$$\Delta W = -\eta \frac{\partial L}{\partial W} = -\eta \frac{\partial L}{\partial v(N)} \frac{\partial v(N)}{\partial W} = \Delta W_U + \sum_{m=0}^{n-2} \sum_{i, j \in N, i \neq j} R^{(m)} \frac{\partial I^{(m)}(i, j)}{\partial W}, \quad (4)$$

where  $U = v(\emptyset) + \sum_{i \in N} \mu_i$ , and  $R^{(m)} = -\eta \frac{\partial L}{\partial v(N)} \frac{\partial v(N)}{\partial I^{(m)}(i, j)}$ . Here,  $\Delta W_U = -\eta \frac{\partial L}{\partial v(N)} \frac{\partial v(N)}{\partial U} \frac{\partial U}{\partial W}$  represents the component of  $\Delta W$  w.r.t.  $\frac{\partial U}{\partial W}$ . Let  $\Delta W^{(m)}(i, j) = R^{(m)} \frac{\partial I^{(m)}(i, j)}{\partial W}$  represent the compositional component of  $\Delta W$  w.r.t.  $\frac{\partial I^{(m)}(i, j)}{\partial W}$ . Therefore, besides  $\Delta W_U$ , we can consider there are additional  $\frac{n(n-1)^2}{2}$  paths w.r.t. different pairs of  $i, j$  in the backpropagation, and the weight change through each propagation path is  $\Delta W^{(m)}(i, j)$ . In this way, we can consider  $\Delta W^{(m)}(i, j)$  measures the strength of learning the average interaction between variables  $i$  and  $j$  under contexts of  $m$  variables.

**Theorem 1.** (Proof in Appendix B) Assume  $\frac{\partial \Delta v(i, j, S)}{\partial W} \sim \mathcal{N}(0, \sigma^2)$ . Then,  $\Delta W^{(m)}(i, j) = R^{(m)} \frac{\partial I^{(m)}(i, j)}{\partial W} \sim \mathcal{N}(0, (\eta \frac{\partial L}{\partial v(N)} w^{(m)})^2 \sigma^2 / \binom{n-2}{m})$ , where  $w^{(m)} = \frac{n-m-1}{n(n-1)}$ .

Theorem 1 shows that the strength  $|\Delta W^{(m)}(i, j)|$  of learning  $m$ -order interactions is proportional to  $F^{(m)} = w^{(m)} / \sqrt{\binom{n-2}{m}} = \frac{n-m-1}{n(n-1)} / \sqrt{\binom{n-2}{m}}$ . Therefore, when the order  $m$  is small or large (e.g.,  $m = 0.05n$  or  $0.95n$ ), the training strength of the  $m$ -order interaction is relatively higher. In contrast, when the order  $m$  is medium (e.g.,  $m = 0.5n$ ), the training strength of the  $m$ -order interaction is much lower. The above analysis explains why it is easy for a DNN to learn low-order and high-order interactions, but difficult for a DNN to learn middle-order interactions.

**Simulation of the curve of the interaction strength.** We find that the above training strength  $|\Delta W^{(m)}(i, j)|$  can be used to simulate the distribution of interaction strengths  $J^{(m)}$  in real applications, which verifies our theory. Based on Theorem 1, the training strength w.r.t. the order  $m$  is proportional to the aforementioned  $F^{(m)}$ , so we can use  $F^{(m)}$  to simulate  $J^{(m)}$ . For fair comparison, we normalize  $F^{(m)}$  and  $J^{(m)}$  by  $\hat{F}^{(m)} = F^{(m)} / F^{(0)}$  and  $\hat{J}^{(m)} = J^{(m)} / J^{(0)}$  respectively, such that  $\hat{F}^{(0)} = \hat{J}^{(0)} = 1$ . As Figure 3(b) shows, the curves of normalized  $\hat{F}^{(m)}$  can well match the distributions of  $\hat{J}^{(m)}$  in real applications. Due to the redundancy of feature representations in DNNs, we usually consider that the actual dimension  $n'$  of the latent space of DNNs is much lower than the number  $n$  of input variables. Therefore, instead of directly using the number  $n$  of input variables, we adopted a smaller  $n'$  (i.e.,  $n' < n$ ) in  $\hat{F}^{(m)}$  for the simulation.

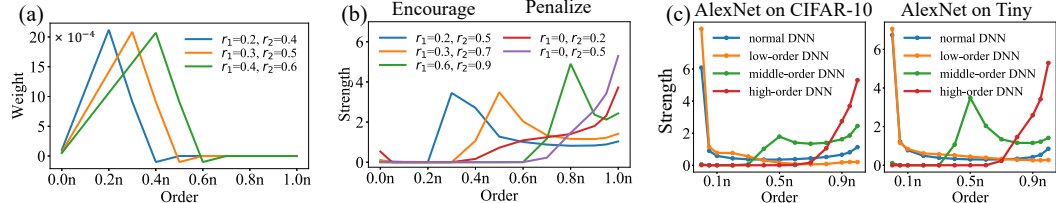


Figure 4: (a) Weight coefficients  $\tilde{w}^{(m)}$  of different orders when we set different pairs of  $(r_1, r_2)$ . (b) Distributions of the interaction strength  $J^{(m)}$  over different orders. Each curve indicates a DNN (using AlexNet) whose interactions were encouraged/penalized by  $L^+$  and  $L^-$  with certain pairs of  $(r_1, r_2)$ . (c) Distributions of the interaction strength  $J^{(m)}$  of four types of DNNs using AlexNet. The Appendix C provides more results.

### 3.3 METHOD TO CONTROL INTERACTIONS OF SPECIFIC ORDERS

The representation bottleneck is widely shared by DNNs of different architectures for various tasks, when DNNs are normally trained. In this section, we mainly explore methods, which force the DNN to learn interactions of specific orders. In this way, we can investigate the properties of feature representations of such DNNs.

In order to force the DNN to learn interactions of specific orders, we propose two simple-yet-efficient losses in the training process. The two losses encourage and penalize interactions of specific orders, respectively. Before designing the two losses, let us focus on the output change  $\Delta v(r_1, r_2)$  between two subsets of variables  $S_1$  and  $S_2$ :

$$\Delta v(r_1, r_2) = v(S_2) - \frac{r_2}{r_1} v(S_1), \quad \text{subject to } \emptyset \subseteq S_1 \subsetneq S_2 \subseteq N \quad (5)$$

where the two subsets  $S_1$  and  $S_2$  are randomly sampled from all input variables  $N$ , such that  $\emptyset \subseteq S_1 \subsetneq S_2 \subseteq N$ ,  $|S_1| = r_1 n$ ,  $|S_2| = r_2 n$ , and  $0 \leq r_1 < r_2 \leq 1$ .

**Theorem 2.** (*Proof in Appendix B*) The output change  $\Delta v(r_1, r_2)$  can be decomposed into the sum of multi-order interactions between different pairs of variables.

$$\Delta v(r_1, r_2) = \left(1 - \frac{r_2}{r_1}\right) v(\emptyset) + \sum_{m=0}^{n-2} \sum_{i,j \in N, i \neq j} \tilde{w}^{(m)} I^{(m)}(i, j)$$

$$\text{where } \tilde{w}^{(m)} = \begin{cases} \frac{(r_2 - 1)(m+1)}{r_1} / [n(n-1)], & m \leq r_1 n - 2 \\ (r_2 n - m - 1) / [n(n-1)], & r_1 n - 2 < m \leq r_2 n - 2 \\ 0, & r_2 n - 2 < m \leq n - 2 \end{cases} \quad (6)$$

Interestingly, as Figure 4(a) shows, we can consider that the output change  $\Delta v(r_1, r_2)$  mainly encodes interactions whose orders are in the range of  $[0, r_2 n]$ . The weight coefficient  $\tilde{w}^{(m)}$  of the  $m$ -th order interaction reached a peak at the  $r_1 n$ -th order in  $\Delta v(r_1, r_2)$ .

**Encourage/penalize interactions of specific orders.** Based on the above analysis,  $\Delta v(r_1, r_2)$  only contains partial interactions of the  $[0, r_2 n]$ -th orders. Hence, we propose two losses based on  $\Delta v(r_1, r_2)$ , which encourage and penalize the DNN to use interactions of specific orders for inference, respectively. The first loss  $L^+$  forces the DNN to mainly use interactions encoded in  $\Delta v(r_1, r_2)$  for inference, thereby boosting the learning of these interactions.

$$L^+ = -\frac{1}{|\Omega|} \sum_{x \in \Omega} \sum_{c=1}^C P(y^* = c|x) \log P(\hat{y} = c|\Delta v_c(r_1, r_2|x)), \quad (7)$$

where  $L^+$  is the proposed cross entropy that uses  $\Delta v(r_1, r_2)$  for classification. Here,  $\Omega$  is the training set, and  $C$  denotes the number of classes. Given an input image  $x \in \Omega$ ,  $y^*$  is the true label, and  $\hat{y}$  denotes the predicted label. Here,  $\Delta v_c(r_1, r_2|x) = v_c(S_2|x) - \frac{r_2}{r_1} v_c(S_1|x)$  denotes the change of the logits of the category  $c$ , where the logit  $v_c(S|x)$  denotes the feature dimension corresponding to the  $c$ -th category before the softmax layer. The two subsets  $S_1, S_2$  are randomly sampled. In this way, we compute  $P(\hat{y} = c|\Delta v_c(r_1, r_2|x))$  as the probability of using the  $C$ -dimensional vector  $\{\Delta v_c(r_1, r_2|x) | 1 \leq c \leq C\}$  to classify the sample to the category  $c$ . We input the  $C$ -dimensional vector  $\{\Delta v_c(r_1, r_2|x) | 1 \leq c \leq C\}$  into the softmax layer to compute the probability.

Table 1: (left) Classification accuracies of four types of DNNs, including the normally trained DNNs, and the other three types of DNNs mainly encoding low-order, middle-order, and high-order interactions. (right) Comparison of adversarial accuracies between normally trained DNNs and DNNs mainly encoding high-order interactions.

Model	CIFAR-10 dataset			Tiny-ImageNet dataset			Model	Normal training	Penalizing low-order & boosting high-order
	AlexNet	VGG16	VGG19	AlexNet	VGG16	VGG19			
Normal training	88.52	90.50	90.61	56.00	56.16	52.56	MLP-5 on census	38.22	<b>7.31</b>
Low interaction	86.97	89.99	89.74	57.52	55.04	55.44	MLP-8 on census	39.33	<b>2.02</b>
Middle interaction	86.65	90.29	90.03	53.88	55.84	53.36	MLP-5 on commercial	27.01	<b>22.00</b>
High interaction	88.68	90.84	90.79	56.12	55.36	53.28	MLP-8 on commercial	25.92	<b>20.58</b>

Besides, the second loss  $L^-$  is designed to prevent the DNN from encoding interactions of the  $[0, r_2n]$ -th orders. Specifically, we maximize the entropy of classification based on  $\Delta v(r_1, r_2)$ , in order to make  $\Delta v(r_1, r_2)$  non-discriminative.

$$L^- = \frac{1}{|\Omega|} \sum_{x \in \Omega} \sum_{c=1}^C P(\hat{y} = c | \Delta v_c(r_1, r_2 | x)) \log P(\hat{y} = c | \Delta v_c(r_1, r_2 | x)), \quad (8)$$

where  $L^-$  denotes the minus entropy of the classification probability based on  $\Delta v_c(r_1, r_2)$ .

In this way, we can train a DNN using the following loss,

$$\text{Loss} = \text{Loss}_{\text{classification}} + \lambda_1 L^+ + \lambda_2 L^- \quad (9)$$

where  $\lambda_1 > 0, \lambda_2 > 0$  are two constants to balance the three terms.

**Effects of the two losses.** We find that the loss  $L^-$  can successfully penalize interactions of  $[0, r_2n]$ -th orders.  $L^+$  can encourage interactions of the  $[r_1n, r_2n]$ -th orders, instead of encouraging interactions of the  $[0, r_2n]$ -th orders. Specifically, we conducted the following experiments. We trained AlexNet networks on the Tiny-ImageNet dataset to encourage interactions of specific orders without penalizing any interactions by setting  $\lambda_1 = 1, \lambda_2 = 0$ . In experiments, we set  $[r_1 = 0.2, r_2 = 0.5]$ ,  $[r_1 = 0.3, r_2 = 0.7]$ , and  $[r_1 = 0.6, r_2 = 0.9]$  in the  $L^+$  loss to learn three AlexNet models, respectively. We also trained AlexNet models to penalize interactions of specific orders by setting  $\lambda_1 = 0, \lambda_2 = 1$ . Two DNNs were trained by setting  $[r_1 = 0, r_2 = 0.2]$  and  $[r_1 = 0, r_2 = 0.5]$  in the  $L^-$  loss, respectively. Figure 4(b) shows the interaction strength  $J^{(m)}$  of these DNNs. When we encouraged the DNN to encode interactions of the  $[r_1n, r_2n]$ -th orders, the interaction strength  $J^{(m)}$  of the  $[r_1n, r_2n]$ -th orders significantly increased, compared to the normally trained DNNs. Figure 4(b) also shows that the loss  $L^-$  could successfully remove interactions of the  $[0, r_2n]$ -th orders.

### 3.4 INVESTIGATION OF THE REPRESENTATION CAPACITIES

In the previous subsection, we introduce two losses, which force the DNN to encode interactions of different orders. In this subsection, we investigate the representation capacities of such DNNs. Thus, we conducted experiments to train four types of DNNs. The first DNN was normally trained. The other three types of DNNs were trained to mainly encode low-order, middle-order, and high-order interactions, respectively. Specifically, the second DNN was trained to penalize interactions of the  $[0.7n, n]$ -th orders by minimizing the  $L^-$  loss with  $\lambda_1 = 0, \lambda_2 = 1, r_1 = 0.7, r_2 = 1.0$ . The third DNN was learned to boost interactions of the  $[0.3n, 0.7n]$ -th orders by minimizing the  $L^+$  loss with  $\lambda_1 = 1, \lambda_2 = 0, r_1 = 0.3, r_2 = 0.7$ . The fourth DNN was trained to penalize interactions of the  $[0, 0.5n]$ -th orders by minimizing the  $L^-$  loss with  $\lambda_1 = 0, \lambda_2 = 1, r_1 = 0, r_2 = 0.5$ . The second DNN, the third DNN, and the fourth DNN were termed *the low-order DNN*, *the middle-order DNN* and *the high-order DNN*, respectively. In experiments, we trained three versions of each DNN based on the above four settings. We applied architectures of AlexNet and VGG-16/19 architectures on the CIFAR-10 and the Tiny-ImageNet dataset.

Figure 4(c) and Figure 7 (in the appendix) show that the trained DNNs successfully learned interactions as expected. In other words, interactions of the  $[0.7n, n]$ -th orders were penalized in the low-order DNN. Interactions of the  $[0.3n, 0.7n]$ -th orders were boosted in the middle-order DNN. Interactions of the  $[0, 0.5n]$ -th orders were penalized in the high-order DNN.

**Classification accuracy.** Firstly, Table 1 shows classification performance of the above four types of DNNs. In general, the four types of DNNs achieved similar accuracies. The similar performance indicated that it was not necessary for a DNN to encode low-order interactions and high-order interactions to make inferences. Middle-order interactions can also provide discriminative information.

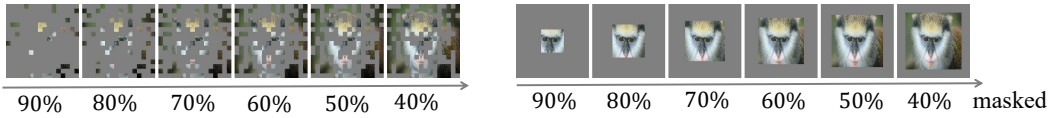


Figure 5: Tested images generated by random masking (left) and surrounding masking (right).

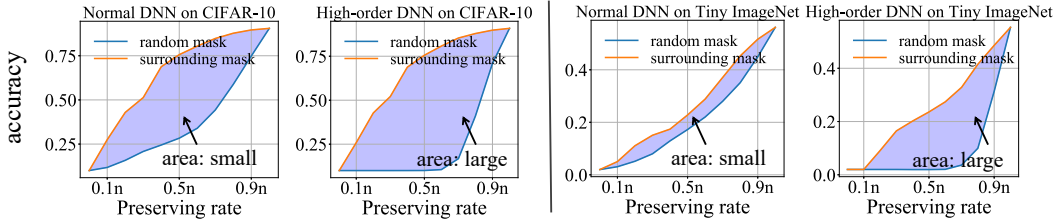


Figure 6: Classification accuracies using VGG-16 on images with different numbers of patches being masked. The Appendix C provides more results.

**Bag-of-words representations vs. structural representations.** Theoretically, high-order interactions usually represent the global structure of objects, which requires the complex collaborations of massive input variables. In comparison, low-order interactions learn local patterns from local and simple collaborations of a few input variables.

Therefore, we conducted two experiments to examine whether the high-order DNN encoded more structural information than the normally trained DNN. Specifically, as Figure 5 shows, in the first experiment, we tested the DNN on images where  $m$  patches in each image were randomly masked. In the second experiment, we tested the DNN on images where  $m$  patches in each image on the image boundary were masked, and the patches in the center were preserved. In this way, we could consider the structural information in tested images was destroyed in the first experiment, but such information was maintained in the second experiment. Here, in each sub-figure in Figure 6, we computed the area between the accuracy curve of randomly masked samples and the accuracy curve of surroundingly masked samples. The area indicated the sensitivity to the structural destruction. We found that such area of high-order DNNs were much larger than the area of normally trained DNNs. This phenomenon indicated that the normally trained DNN usually encoded local patterns, just like the bag-of-words representations, which were robust to the structural destruction. However, high-order DNN encoded more structural information.

**Adversarial robustness.** Ren et al. (2021) have demonstrated that adversarial attacks mainly affect high-order interactions. Therefore, we conducted experiments to train DNNs mainly encoding high-order interactions based on the proposed losses, in order to verify whether such DNNs were more vulnerable to adversarial attacks. To train DNNs mainly encoding high-order interactions, we trained DNNs by setting  $\lambda_1 = 1, \lambda_2 = 1$ . Specifically, the DNN was trained to encourage interactions of the  $[0.6n, n]$ -th orders by setting  $r_1 = 0.6, r_2 = 1$  for  $L^+$  and simultaneously penalize interactions of the  $[0, 0.5n]$ -th orders by setting  $r'_1 = 0, r'_2 = 0.5$  for  $L^-$  simultaneously. We used the aforementioned MLP-5 and MLP-8 networks in section 3.1. Each MLP was trained on the census and commercial dataset, respectively. Figure 9 in the appendix shows distributions of interaction strength of these DNNs. Then, we compared the adversarial robustness between normally trained DNNs and the DNNs whose high-order interactions were boosted. We adopted the untargeted PGD attack (Madry et al., 2018) based on  $L_\infty$  norm. We set the attack strength  $\epsilon = 0.6$  with 100 steps for the census dataset, and set  $\epsilon = 0.2$  with 50 steps for the commercial dataset. The step size was uniformly set to 0.01 for all attacks. Please see more implementation details in Appendix C. Table 1 shows that DNNs with the boosted high-order interactions exhibited significantly lower adversarial accuracies than normally trained DNN, especially on the census dataset. These results verified that high-order interactions were vulnerable to adversarial attacks.

## 4 CONCLUSION

In this paper, we have discovered and theoretically proved the representation bottleneck of DNNs, from a new perspective of the complexity of interactions encoded in DNNs. We adopt the multi-order interaction, and we use the order to represent the complexity of interactions. It is a common

phenomenon that a DNN usually encodes very simple interactions and very complex interactions, but rarely learns interactions of intermediate complexity. We have theoretically proved the underlying reason for the representation bottleneck. Furthermore, we propose two losses to learn DNNs which encode interactions of specific complexities. Experimental results have shown that it is not necessary for a DNN to encode or avoid encoding interactions of specific orders, in terms of classification performance. However, high-order interactions usually encode more structural information than low-order interactions, and are usually vulnerable to adversarial attacks.

## ACKNOWLEDGMENTS

This work is partially supported by the National Nature Science Foundation of China (No. 61906120, U19B2043), Shanghai Natural Science Fundation (21JC1403800,21ZR1434600), Shanghai Municipal Science and Technology Major Project (2021SHZDZX0102). This work is also partially supported by Huawei Technologies Inc.

## REFERENCES

Alessandro Achille and Stefano Soatto. Information dropout: Learning optimal representations through noisy computation. *IEEE transactions on pattern analysis and machine intelligence*, 40(12):2897–2905, 2018.

Rana Ali Amjad and Bernhard C Geiger. Learning representations for neural network-based classification using the information bottleneck principle. *IEEE transactions on pattern analysis and machine intelligence*, 42(9):2225–2239, 2019.

Marco Ancona, Cengiz Oztireli, and Markus Gross. Explaining deep neural networks with a polynomial time algorithm for shapley value approximation. In *International Conference on Machine Learning*, pp. 272–281. PMLR, 2019.

Devansh Arpit, Stanislaw Jastrzkebski, Nicolas Ballas, David Krueger, Emmanuel Bengio, Maxinder S Kanwal, Tegan Maharaj, Asja Fischer, Aaron Courville, Yoshua Bengio, et al. A closer look at memorization in deep networks. In *International Conference on Machine Learning*, pp. 233–242. PMLR, 2017.

Dheeru Dua, Casey Graff, et al. Uci machine learning repository. 2017.

Stanislav Fort, Paweł Krzysztof Nowak, Stanislaw Jastrzebski, and Srini Narayanan. Stiffness: A new perspective on generalization in neural networks. *arXiv preprint arXiv:1901.09491*, 2019.

Michel Grabisch and Marc Roubens. An axiomatic approach to the concept of interaction among players in cooperative games. *International Journal of game theory*, 28(4):547–565, 1999.

Kaiming He, Xiangyu Zhang, Shaoqing Ren, and Jian Sun. Deep residual learning for image recognition. In *Proceedings of the IEEE conference on computer vision and pattern recognition*, pp. 770–778, 2016.

R Devon Hjelm, Alex Fedorov, Samuel Lavoie-Marchildon, Karan Grewal, Phil Bachman, Adam Trischler, and Yoshua Bengio. Learning deep representations by mutual information estimation and maximization. In *International Conference on Learning Representations*, 2019.

Joseph D Janizek, Pascal Sturmels, and Su-In Lee. Explaining explanations: Axiomatic feature interactions for deep networks. *Journal of Machine Learning Research*, 22(104):1–54, 2021.

Alex Krizhevsky, Geoffrey Hinton, et al. Learning multiple layers of features from tiny images. 2009.

Alex Krizhevsky, Ilya Sutskever, and Geoffrey E Hinton. Imagenet classification with deep convolutional neural networks. In *Advances in Neural Information Processing Systems*, volume 25, pp. 1097–1105, 2012.

Ya Le and Xuan Yang. Tiny imagenet visual recognition challenge. *CS 231N*, 7(7):3, 2015.

Benjamin Lengerich, Eric P Xing, and Rich Caruana. On dropout, overfitting, and interaction effects in deep neural networks. *arXiv preprint arXiv:2007.00823*, 2020.

Jianxun Lian, Xiaohuan Zhou, Fuzheng Zhang, Zhongxia Chen, Xing Xie, and Guangzhong Sun. xdeepfm: Combining explicit and implicit feature interactions for recommender systems. In *Proceedings of the 24th ACM SIGKDD International Conference on Knowledge Discovery & Data Mining*, pp. 1754–1763, 2018.

Scott M Lundberg and Su-In Lee. A unified approach to interpreting model predictions. In *Proceedings of the 31st international conference on neural information processing systems*, pp. 4768–4777, 2017.

Scott M Lundberg, Gabriel G Erion, and Su-In Lee. Consistent individualized feature attribution for tree ensembles. *arXiv preprint arXiv:1802.03888*, 2018.

Aleksander Madry, Aleksandar Makelov, Ludwig Schmidt, Dimitris Tsipras, and Adrian Vladu. Towards deep learning models resistant to adversarial attacks. In *International Conference on Learning Representations*, 2018.

Guido Montúfar, Razvan Pascanu, Kyunghyun Cho, and Yoshua Bengio. On the number of linear regions of deep neural networks. In *Advances in Neural Information Processing Systems*, 2014.

Behnam Neyshabur, Srinadh Bhojanapalli, David McAllester, and Nathan Srebro. Exploring generalization in deep learning. In *Advances in Neural Information Processing Systems*, 2017.

Roman Novak, Yasaman Bahri, Daniel A Abolafia, Jeffrey Pennington, and Jascha Sohl-Dickstein. Sensitivity and generalization in neural networks: an empirical study. *arXiv preprint arXiv:1802.08760*, 2018.

Razvan Pascanu, Guido Montufar, and Yoshua Bengio. On the number of response regions of deep feed forward networks with piece-wise linear activations. *arXiv preprint arXiv:1312.6098*, 2013.

William Peebles, John Peebles, Jun-Yan Zhu, Alexei Efros, and Antonio Torralba. The hessian penalty: A weak prior for unsupervised disentanglement. In *Computer Vision–ECCV 2020: 16th European Conference, Glasgow, UK, August 23–28, 2020, Proceedings, Part VI 16*, pp. 581–597. Springer, 2020.

Jie Ren, Die Zhang, Yisen Wang, Lu Chen, Zhanpeng Zhou, Xu Cheng, Xin Wang, Yiting Chen, Jie Shi, and Quanshi Zhang. Game-theoretic understanding of adversarially learned features. *arXiv preprint arXiv:2103.07364*, 2021.

Olga Russakovsky, Jia Deng, Hao Su, Jonathan Krause, Sanjeev Satheesh, Sean Ma, Zhiheng Huang, Andrej Karpathy, Aditya Khosla, Michael Bernstein, Alexander C. Berg, and Li Fei-Fei. ImageNet Large Scale Visual Recognition Challenge. *International Journal of Computer Vision (IJCV)*, 115(3):211–252, 2015. doi: 10.1007/s11263-015-0816-y.

LS Shapley. Notes on the n-person game—ii: The value of an n-person game, the rand corporation, the rand corporation. *Research Memorandum*, 670, 1951.

Ravid Shwartz-Ziv and Naftali Tishby. Opening the black box of deep neural networks via information. *arXiv preprint arXiv:1703.00810*, 2017.

Karen Simonyan and Andrew Zisserman. Very deep convolutional networks for large-scale image recognition. In *International Conference on Learning Representations*, 2014.

Weiping Song, Chence Shi, Zhiping Xiao, Zhijian Duan, Yewen Xu, Ming Zhang, and Jian Tang. Autoint: Automatic feature interaction learning via self-attentive neural networks. In *Proceedings of the 28th ACM International Conference on Information and Knowledge Management*, pp. 1161–1170, 2019.

Mukund Sundararajan, Ankur Taly, and Qiqi Yan. Axiomatic attribution for deep networks. In *International Conference on Machine Learning*, pp. 3319–3328. PMLR, 2017.

Mukund Sundararajan, Kedar Dhamdhere, and Ashish Agarwal. The shapley taylor interaction index. In *International Conference on Machine Learning*, pp. 9259–9268. PMLR, 2020.

Michael Tsang, Dehua Cheng, and Yan Liu. Detecting statistical interactions from neural network weights. In *International Conference on Learning Representations*, 2017.

Michael Tsang, Hanpeng Liu, Sanjay Purushotham, Pavankumar Murali, and Yan Liu. Neural interaction transparency (nit): Disentangling learned interactions for improved interpretability. *Advances in Neural Information Processing Systems*, 31:5804–5813, 2018.

Michael Tsang, Dehua Cheng, Hanpeng Liu, Xue Feng, Eric Zhou, and Yan Liu. Feature interaction interpretability: A case for explaining ad-recommendation systems via neural interaction detection. In *International Conference on Learning Representations*, 2020.

Tsui-Wei Weng, Huan Zhang, Pin-Yu Chen, Jinfeng Yi, Dong Su, Yupeng Gao, Cho-Jui Hsieh, and Luca Daniel. Evaluating the robustness of neural networks: An extreme value theory approach. *arXiv preprint arXiv:1801.10578*, 2018.

Zhiqin John Xu. Understanding training and generalization in deep learning by fourier analysis. *arXiv preprint arXiv:1808.04295*, 2018.

Hao Zhang, Sen Li, Yinchen Ma, Mingjie Li, Yichen Xie, and Quanshi Zhang. Interpreting and boosting dropout from a game-theoretic view. In *International Conference on Learning Representations*, 2020.

## A THE MULTI-ORDER INTERACTION

Zhang et al. (2020) proposed the multi-order interaction between input variables  $i, j$  as follows:

$$I^{(m)}(i, j) = \mathbb{E}_{|S| \subseteq N \setminus \{i, j\}, |S|=m} \Delta v(i, j, S)$$

where  $\Delta v(i, j, S) = v(S \cup \{i, j\}) - v(S \cup \{i\}) - v(S \cup \{j\}) + v(S)$ .  $I^{(m)}(i, j)$  denotes the interaction between variables  $i, j \in N$  of the  $m$ -th order, which measures the average interaction utility between  $i, j$  under contexts of  $m$  variables. It has been proven that  $I^{(m)}(i, j)$  satisfies the following five desirable properties.

- **Linear property.** If two independent games  $u$  and  $v$  are combined,  $w(S) = u(S) + v(S)$ , then the multi-order interaction of the combined game equals to the sum of multi-order interactions derived from  $u$  and  $v$ . *I.e.*,  $I_w^{(m)}(i, j) = I_u^{(m)}(i, j) + I_v^{(m)}(i, j)$ .
- **Nullity property.** A dummy variable  $i \in N$  satisfies  $\forall S \subseteq N \setminus \{i\}, v(S \cup \{i\}) = v(S) + v(\{i\})$ . Then, variable  $i$  has no interactions with other variables, *i.e.*,  $\forall m, \forall j \in N \setminus \{i\}, I^{(m)}(i, j) = 0$ .
- **Commutativity property.**  $\forall i, j \in N, I^{(m)}(i, j) = I^{(m)}(j, i)$ .
- **Symmetry property.** Assume two variables  $i, j$  are equivalent in the sense that  $i, j$  have same cooperations with other variables,  $\forall S \subseteq N \setminus \{i, j\}, v(S \cup \{i\}) = v(S \cup \{j\})$ . Then, for any variable  $k \in N, I^{(m)}(i, k) = I^{(m)}(j, k)$ .
- **Efficiency property.** The network output of a DNN can be decomposed into the sum of interactions of different orders between different pairs of variables.

$$v(N) - v(\emptyset) = \sum_{i \in N} \mu_i + \sum_{i, j \in N, i \neq j} \sum_{m=0}^{n-2} w^{(m)} I^{(m)}(i, j).$$

where  $\mu_i = v(\{i\}) - v(\emptyset)$  represents the independent effect of variable  $i$ , and  $w^{(m)} = \frac{n-1-m}{n(n-1)}$ .

### Connection with Shapley value and Shapley interaction index.

*Shapley value.* Shapley (1951) proposed the Shapley value to measure the numerical importance of each player to the total reward in a cooperative game. The Shapley value has been widely used to explain the decision of DNNs in recent years (Lundberg & Lee, 2017; Ancona et al., 2019). For a given DNN and an input sample with a set of input variables  $N = \{1, \dots, n\}$ , we use  $2^N = \{S | S \subseteq N\}$  to denote all possible variable subsets of  $N$ . Then, the DNN  $v$  can be considered as  $v : 2^N \rightarrow \mathbb{R}$  that calculates the output  $v(S)$  of each specific subset  $S \subseteq N$ . Each input variable  $i$  is regarded as a player, and the network output  $v(N)$  of all input variables can be considered as the total reward of the game. The Shapley value aims to fairly distribute the network output to each individual variables as follows:

$$\phi_i = \sum_{S \subseteq N \setminus \{i\}} \frac{|S|!(n-|S|-1)!}{n!} [v(S \cup \{i\}) - v(S)]$$

where  $v(S)$  denotes the network output when we keep variables in  $S$  unchanged while mask variables in  $N \setminus S$  by following the setting in Ancona et al. (2019). It has been proven that the Shapley value is an unique method to fairly allocate overall reward to each player that satisfies *linearity*, *nullity*, *symmetry*, and *efficiency* properties.

*Connections between the Shapley interaction index and the Shapley value.* Input variables of a DNN usually interact with each other, instead of working individually. Based on the Shapley value, Grabisch & Roubens (1999) further proposed the Shapley interaction index to measure the interaction utility between input variables. The Shapley interaction index is the only axiomatic extension of the Shapley value, which satisfies *linearity*, *nullity*, *symmetry*, and *recursive* properties. For two variables  $i, j \in N$ , the Shapley interaction index  $I(i, j)$  can be considered as the change of the numerical importance of variable  $i$  by the presence or absence of variable  $j$ .

$$I(i, j) = \tilde{\phi}(i)_{j \text{ always present}} - \tilde{\phi}(i)_{j \text{ always absent}},$$

where  $\tilde{\phi}(i)_{j \text{ always present}}$  denotes the Shapley value of the variable  $i$  computed under the specific condition that variable  $j$  is always present.  $\tilde{\phi}(i)_{j \text{ always absent}}$  is computed under the specific condition that  $j$  is always absent.

*Connections between the multi-order interaction and the Shapley interaction index.* Based on the Shapley interaction index, Zhang et al. (2020) further defined the order of interaction, which represents the contextual complexity of interactions. It has been proven that the above Shapley interaction index  $I(i, j)$  between variables  $i, j$  can be decomposed into multi-order interactions as follows:

$$I(i, j) = \frac{1}{n-1} \sum_{m=0}^{n-2} I^{(m)}(i, j).$$

## B PROOF OF THEOREMS

**Motivation of Theorem 1.** Let  $W$  denote network parameters of the DNN. Let  $L$  and  $\eta$  denote the loss function and learning rate of training, respectively. According to the efficiency property of  $I^{(m)}(i, j)$  in Eq. (2), the network output  $v(N)$  of a DNN can be decomposed into the sum of multi-order interactions  $I^{(m)}(i, j)$ . Therefore, the change of weights  $\Delta W$  can be computed by:

$$\begin{aligned} \Delta W &= -\eta \frac{\partial L}{\partial W} = -\eta \frac{\partial L}{\partial v(N)} \frac{\partial v(N)}{\partial W} = \Delta W_U + \sum_{m=0}^{n-2} \sum_{i,j \in N, i \neq j} R^{(m)} \frac{\partial I^{(m)}(i, j)}{\partial W} \\ \text{where } U &= v(\emptyset) + \sum_{i \in N} \mu_i, \Delta W_U = -\eta \frac{\partial L}{\partial v(N)} \frac{\partial v(N)}{\partial U} \frac{\partial U}{\partial W}, \\ R^{(m)} &= -\eta \frac{\partial L}{\partial v(N)} \frac{\partial v(N)}{\partial I^{(m)}(i, j)}. \end{aligned}$$

Based on the analysis in section 3.2,  $\Delta W^{(m)}(i, j) = R^{(m)} \frac{\partial I^{(m)}(i, j)}{\partial W}$  represents the strength of learning the average interaction between variables  $i$  and  $j$  under contexts of  $m$  variables. Therefore, in Theorem 1, we aim to prove that the learning strength  $\Delta W^{(m)}(i, j) \sim \mathcal{N}(0, (\eta \frac{\partial L}{\partial v(N)} w^{(m)})^2 \sigma^2 / \binom{n-2}{m})$ .

**Proof of Theorem 1.** The  $m$ -order interaction  $I^{(m)}(i, j)$  between variables  $i, j$  is defined as,

$$\begin{aligned} I^{(m)}(i, j) &= \mathbb{E}_{S \subseteq N \setminus \{i, j\}, |S|=m} \Delta v(i, j, S) \\ &= \frac{1}{\binom{n-2}{m}} \sum_{\substack{S \subseteq N \setminus \{i, j\} \\ |S|=m}} \Delta v(i, j, S). \end{aligned} \tag{10}$$

Assume  $\frac{\partial \Delta v(i, j, S)}{\partial W} \sim \mathcal{N}(0, \sigma^2)$ . Based on Eq. (10), we have,

$$\begin{aligned} \frac{\partial I^{(m)}(i, j)}{\partial W} &= \sum_{\substack{S \subseteq N \setminus \{i, j\} \\ |S|=m}} \frac{\partial I^{(m)}(i, j)}{\partial \Delta v(i, j, S)} \frac{\partial \Delta v(i, j, S)}{\partial W} \\ &= \frac{1}{\binom{n-2}{m}} \sum_{\substack{S \subseteq N \setminus \{i, j\} \\ |S|=m}} \frac{\partial \Delta v(i, j, S)}{\partial W} \sim \mathcal{N}(0, \frac{1}{\binom{n-2}{m}} \sigma^2) \end{aligned}$$

Therefore,  $\Delta W^{(m)}(i, j) = R^{(m)} \frac{\partial I^{(m)}(i, j)}{\partial W} \sim \mathcal{N}(0, \frac{(R^{(m)})^2}{\binom{n-2}{m}} \sigma^2)$ . Since the efficiency property in Eq.

2 shows that  $\frac{\partial v(N)}{\partial I^{(m)}(i, j)} = w^{(m)} = \frac{n-m-1}{n(n-1)}$ , we further obtain that,

$$\Delta W^{(m)}(i, j) \sim \mathcal{N}(0, (\eta \frac{\partial L}{\partial v(N)} w^{(m)})^2 \sigma^2 / \binom{n-2}{m})$$

Then, the conclusion holds.

**Proof of Theorem 2.** Let  $S_1, S_2$  denote the two variable subsets randomly sampled from all input variables  $N$ , where  $|S_1| = r_1 n, |S_2| = r_2 n$ , and  $0 \leq r_1 < r_2 \leq 1$ . According to the efficiency property of the multi-order interaction, we have,

$$\begin{aligned} v(S_1) - v(\emptyset) &= \sum_{i \in S_1} \mu_i + \sum_{i,j \in S_1, i \neq j} \left[ \sum_{m=0}^{r_1 n - 2} \frac{r_1 n - 1 - m}{r_1 n (r_1 n - 1)} I_{S_1}^{(m)}(i, j) \right] \\ &= r_1 n \mathbb{E}_i(\mu_i) + \sum_{m=0}^{r_1 n - 2} \frac{r_1 n - 1 - m}{r_1 n (r_1 n - 1)} \sum_{i,j \in S_1, i \neq j} I_{S_1}^{(m)}(i, j) \\ &= r_1 n \mathbb{E}_i(\mu_i) + \sum_{m=0}^{r_1 n - 2} (r_1 n - 1 - m) \mathbb{E}_{i,j}(I_{S_1}^{(m)}(i, j)) \end{aligned}$$

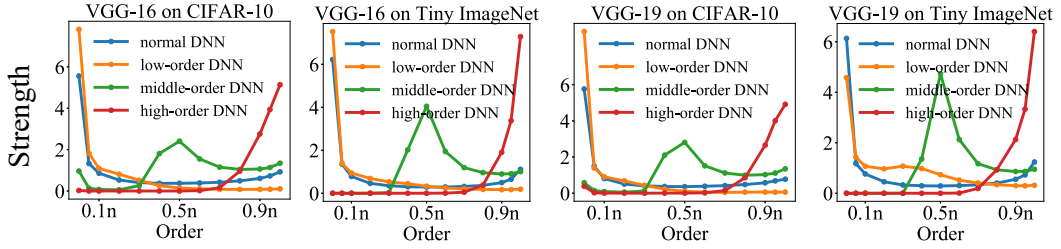
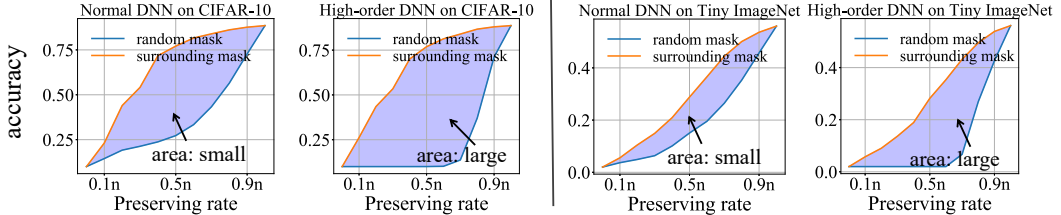
Figure 7: Distributions of the interaction strength  $J^{(m)}$  of four types of DNNs

Figure 8: Classification accuracies using AlexNet on images with different numbers of patches being masked.

where  $I_{S_1}^{(m)}(i, j) \stackrel{\text{def}}{=} \mathbb{E}_{S' \subseteq S_1 \setminus \{i, j\}, |S'|=m}(\Delta v(i, j, S'))$ . Similarly,

$$\begin{aligned} v(S_2) - v(\emptyset) &= \sum_{i \in S_2} \mu_i + \sum_{i, j \in S_2, i \neq j} \left[ \sum_{m=0}^{r_2 n - 2} \frac{r_2 n - 1 - m}{r_2 n (r_2 n - 1)} I_{S_2}^{(m)}(i, j) \right] \\ &= r_2 n \mathbb{E}_i(\mu_i) + \sum_{m=0}^{r_2 n - 2} (r_2 n - 1 - m) \mathbb{E}_{i, j}(I_{S_2}^{(m)}(i, j)) \end{aligned}$$

where  $I_{S_2}^{(m)}(i, j) \stackrel{\text{def}}{=} \mathbb{E}_{S' \subseteq S_2 \setminus \{i, j\}, |S'|=m}(\Delta v(i, j, S'))$ . Note that the contexts when computing  $I_{S_1}^{(m)}(i, j)$  and  $I_{S_2}^{(m)}(i, j)$  are different. Since we can approximately consider that  $\mathbb{E}_{i, j}(I_{S_1}^{(m)}(i, j)) = \mathbb{E}_{i, j}(I_{S_2}^{(m)}(i, j)) = \mathbb{E}_{i, j}(I^{(m)}(i, j))$ ,  $\Delta v(r_1, r_2) = v(S_2) - \frac{r_2}{r_1} v(S_1)$  can be rewritten as:

$$\begin{aligned} \Delta v(r_1, r_2) &= v(S_2) - \frac{r_2}{r_1} v(S_1) \\ &= (1 - \frac{r_2}{r_1}) v(\emptyset) + \sum_{m=0}^{n-2} \sum_{i, j \in N, i \neq j} \tilde{w}^{(m)} I^{(m)}(i, j) \\ \text{where } \tilde{w}^{(m)} &= \begin{cases} (\frac{r_2}{r_1} - 1)(m+1)/[n(n-1)], & m \leq r_1 n - 2 \\ (r_2 n - m - 1)/[n(n-1)], & r_1 n - 2 < m \leq r_2 n - 2 \\ 0, & r_2 n - 2 < m \leq n - 2 \end{cases} \end{aligned}$$

Then, the conclusion holds.

## C EXPERIMENTAL DETAILS AND RESULTS

### C.1 IMPLEMENTATION DETAILS

**The sampling strategy when computing  $J^{(m)}$ .** The interaction strength  $J^{(m)}$  is defined as,

$$J^{(m)} = \frac{\mathbb{E}_{x \in \Omega} [\mathbb{E}_{i, j} [|I^{(m)}(i, j|x)|]]}{\mathbb{E}_{m'} [\mathbb{E}_{x \in \Omega} [\mathbb{E}_{i, j} [|I^{(m')}(i, j|x)|]]]}, \text{ where } I^{(m)}(i, j|x) = \mathbb{E}_{S \subseteq N \setminus \{i, j\}} [\Delta v(i, j, S)].$$

To precisely compute  $J^{(m)}$ , we need to average all possible contexts  $S \subseteq N$ , all pairs of variables  $i, j \in N$ , and all samples  $x \in \Omega$ , which is usually computationally infeasible. Therefore, we computed  $J^{(m)}$  approximately by a sampling strategy (Zhang et al., 2020).

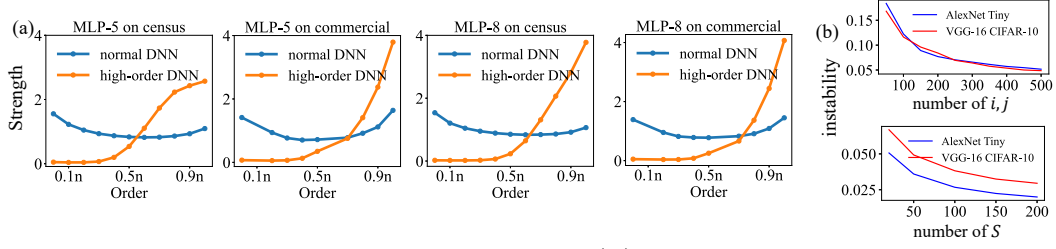


Figure 9: (a) Distributions of the interaction strength  $J^{(m)}$  of normal DNNs and high-order DNNs trained to encourage high-order interactions and penalize low-order interactions simultaneously. (b) The instability of  $J^{(m)}(x)$  w.r.t. the sampling number of pairs of variables  $(i, j)$  and the sampling number of contexts  $S$ .

On each image dataset, we first sampled 50 correctly classified images in total. On the ImageNet and Tiny-ImageNet dataset, these images were sampled from different 50 classes. On the CIFAR-10 dataset, we sampled 5 images from each class. Then, for each image, we sampled 200 pairs of patches  $i, j \in N$ . Since DNNs usually encode stronger interactions between neighbor patches, we restricted that patch  $i$  is located at the neighbor patch  $j$  with a radius of two patches. Next, for each pair of patches  $i, j$  and each order  $m$ , we randomly sampled 100 contexts  $S$  from all possible contexts, where  $|S| = m$ . To plot the curve of interaction strength, we computed 13 orders for  $J^{(m)}$ , where  $m = \frac{r}{10}n, 0 \leq r \leq n$  and  $m = 0.05n, 0.95n$ . On each tabular dataset, since there are only a few input variables ( $n = 12$  on census and  $n = 10$  on commercial), we sampled all 100 instances and all pairs of variables for computation. For each pair of patches  $i, j \in N$  and each order  $m$ , we randomly sampled 100 contexts  $S$  from all possible contexts.

Considering the randomness in the sampling process, we also conducted an experiment to evaluate the stability of the estimated interaction strength  $J^{(m)}$  via the sampling-based approximation method. Specifically, given an input image  $x$  and a sampling number  $q$ , we measured the instability of  $J^{(m)}(x)$ , when we repeatedly computed the interaction for  $q$  times. The instability w.r.t.  $J^{(m)}(x)$  was computed as  $\frac{\mathbb{E}_{u,v;u \neq v} |J_u^{(m)}(x) - J_v^{(m)}(x)|}{\mathbb{E}_w |J_w^{(m)}(x)|}$ , where  $J_u^{(m)}(x), J_v^{(m)}(x)$  denotes the estimated  $J^{(m)}(x)$  at the  $u$ -th sampling time and the  $v$ -th sampling time, respectively. Then, the instability value was computed by averaging over 50 images and all sampled orders, i.e.,  $instability = \mathbb{E}_{x \in \Omega} \mathbb{E}_m [\frac{\mathbb{E}_{u,v;u \neq v} |J_u^{(m)}(x) - J_v^{(m)}(x)|}{\mathbb{E}_w |J_w^{(m)}(x)|}]$ . We used the trained AlexNet on the Tiny-ImageNet dataset and VGG-16 on the CIFAR-10 dataset to compute the instability.

We aim to evaluate how the estimated  $J^{(m)}$  value will be affected by the randomness in the sampling process. During the sampling process to compute  $J^{(m)}(x)$ , we need to sample over multiple pairs of variables  $(i, j)$  and multiple contexts  $S$ . Therefore, we first fixed 100 pairs of  $(i, j)$ , and evaluated the instability of  $J^{(m)}(x)$  w.r.t. the sampling of the contexts  $S$ . Figure 9(b) shows that on the two datasets, when the sampling number of  $S$  increased, the instability decreased. Furthermore, when the sampling number of  $S$  was greater than 100 (i.e., our setting), the instability value was less than 0.05, which indicated a stable approximation. Secondly, we evaluated the instability w.r.t. the sampling processes of  $(i, j)$ , where the sampling number of  $S$  was set to 100 as mentioned above. As Figure 9(b) shows, when the sampling number of  $(i, j)$  pairs increased, the instabilities decreased. When the sampling number of  $(i, j)$  pairs was greater than 200 (i.e., our setting), the instability was less than 0.1, which indicated a stable approximation of  $J^{(m)}(x)$ . These results demonstrated that our sampling strategy can well approximate the interaction strength  $J^{(m)}$ .

**Implementation details of adversarial attacks.** Here, we introduce how to measure the adversarial robustness in section 3.4. We adopted the untargeted PGD attack (Madry et al., 2018) with the  $L_\infty$  constraint  $\|\Delta x\|_\infty \leq \epsilon$  to generate adversarial examples. For the census dataset, we set  $\epsilon = 0.6$  and the attack was conducted with 100 steps. For the commercial dataset, we set  $\epsilon = 0.2$  and the attack was conducted with 50 steps. The step size was set to 0.01 for all attacks.

## C.2 MORE EXPERIMENTAL RESULTS.

In this subsection, we provide more experimental results besides the results in the main paper. Due to the computational cost, when we trained DNNs on the Tiny ImageNet dataset, we selected 50 object classes from 200 classes at equal intervals for training and testing. Figure 7 shows the distributions of  $J^{(m)}$  of four types of DNNs (using VGG-16 and VGG-19) mentioned in section 3.4. The distributions of  $J^{(m)}$  in Figure 7 are consistent with the one in Figure 4(c) of AlexNet model, which further demonstrates that these DNNs could successfully learn interactions as expected. Figure 8 shows the classification accuracies using AlexNet network on images with different numbers of patches being masked. These results further verifies that high-order DNNs were more sensitive to the destruction of structural information. Figure 9 shows the  $J^{(m)}$  distributions of normal DNNs and high-order DNNs on two tabular datasets.